Nanocluster Self-Assembly

DOI: 10.1002/anie.201407390

Colloidal Self-Assembly of Catalytic Copper Nanoclusters into Ultrathin Ribbons**

Zhennan Wu, Yanchun Li, Jiale Liu, Zhongyuan Lu, Hao Zhang, and Bai Yang*

Abstract: *Metal nanoclusters (NCs) with diameter below 2 nm are promising catalysts in oxygen reduction reactions (ORR). However, the high surface energy of ultra-small clusters leads to structural instability, shedding doubt on practical applications. Herein, we demonstrate a self-assembly method to improve the durability of catalytic metal NCs, employing copper NCs capped by 1-dodecanethiol (DT) to form free-standing ribbons in colloidal solution. By tuning the cooperation between the dipolar attraction between Cu NCs and the van der Waals attraction between DT, the thickness of ribbons is adjusted to a single NC scale. Such free-standing ribbons exhibit excellent catalytic activity and durability in ORR.*

Metallic nanomaterials are promising electrocatalysts in oxygen reduction reactions (ORR), which are potentially applicable in green-energy conversion or storage systems ranging from fuel cells to metal–air batteries.[1] Despite the high catalytic activity of noble-metal nanomaterials, the practical applications suffer from high cost, limited reserves, and poor durability, thus motivating interest in developing non-noble-metal nanocatalysts.[2] One alternative material copper, which is both inexpensive and abundant. As Cu can be used to fabricate nanoclusters (NCs) with a diameter of less than 2 nm, the high fraction of low-coordinated surface atoms greatly facilitate oxygen adsorption, thereby enhancing the electrocatalytic performance in comparison to bulk and larger nanometer-sized counterparts.[1b–c,3] To date, however, limited studies have focused on Cu NC-based ORR electrocatalysts, because of Cu NCs can be easily oxidized.[1c,4] In addition, the ultra-small NCs have a high surface energy, leading to aggregation and further fusion of NCs during catalytic reaction.[1b,3b] Such structural instability greatly limits the application of Cu NCs as electrocatalysts.

Self-assembly controls the organization of nanometer-sized building blocks, allowing the preparation of specific architectures, and the resulting structures are expected to show enhanced performances.[5] Herein, we demonstrate the controlled self-assembly of Cu NCs into ultrathin ribbons in colloidal solution, which significantly enhances the structural stability but does not lower the catalytic activity. Cu NCs are prepared using 1-dodecanethiol (DT) to reduce copper(II) acetylacetonate ($CuAc_2$) in a solvent mixture of dibenzyl ether (BE) and liquid paraffin (LP). DT also acts as the capping ligand, leading to the generation of $Cu_{12}DT_8Ac_4$ NCs. The subsequent self-assembly is initiated by the dipolar attraction of $Cu_{12}DT_8Ac$ NCs and is reinforced by their van der Waals (vdW) attraction caused by the DT capping ligands, which produces preassembled nanowires (NWs) with an average diameter of 26 nm, denoted Wire-26. Further annealing treatment converts $Cu_{12}DT_8Ac_4$ into Cu_8DT_8, and breaks the equilibrium between dipolar and vdW attraction. The Cu NCs are rearranged within Wire-26 to produce 1.3 nm thick ribbons, denoted Ribbon-1.3, which is the diameter of a single Cu NC (Figure 1). Such ribbons with single NC thickness maintain the high specific surface areas of Cu NCs and simultaneously improve the durability when employed as electrocatalysts for ORR.

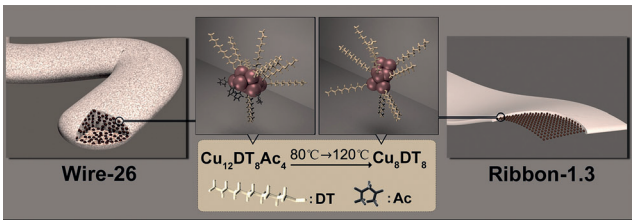

Figure 1. Evolution of Cu NC self-assembly architectures from Wire-26 to Ribbon-1.3. The composition of the material changes from $Cu_{12}DT_8Ac_4$ to Cu_8DT_8.

The preassembly of Wire-26 is performed through a colloidal self-assembly method. In a typical experiment, $CuAc_2$ (30 mg; 0.1 mmol) is dissolved in a mixture of BE (2 mL) and LP (5 mL). Subsequently, DT (1 mL; 4 mmol), which acts both as a ligand and a reductant, is added and heated at 80 °C for 2 minutes under magnetic stirring. Transmission electron microscopy (TEM) images of the resulting product show that the products are ultra-long NWs with an approximate width of 50–120 nm and a length of about 10–20 μm (Figure 2a). The higher magnification image (Figure 2b and Figure S1 in the Supporting Information) clearly show that the building blocks are individual NCs with an average diameter of 1.9 nm. Tapping-mode atomic force microscopy (AFM) reveals that the diameter of the NWs is approximately 26 nm (Figure 2d and Figure S2 in the Supporting Information). This is

[*] Z. N. Wu, J. L. Liu, Prof. H. Zhang, Prof. B. Yang
State Key Laboratory of Supramolecular Structure and Materials
College of Chemistry, Jilin University
Changchun 130012 (P. R. China)
E-mail: hao_zhang@jlu.edu.cn
Dr. Y. C. Li, Prof. Z. Y. Lu
State Key Laboratory of Theoretical and Computational Chemistry
Institute of Theoretical Chemistry, Jilin University
Changchun 130023 (P. R. China)

[**] This work was supported by the 973 Program of China (2014CB643503), NSFC (51425301, 21374042, 21174051, 21221063, 91123031), and the Special Project from MOST of China.
Supporting information for this article is available on the WWW under http://dx.doi.org/10.1002/anie.201407390.

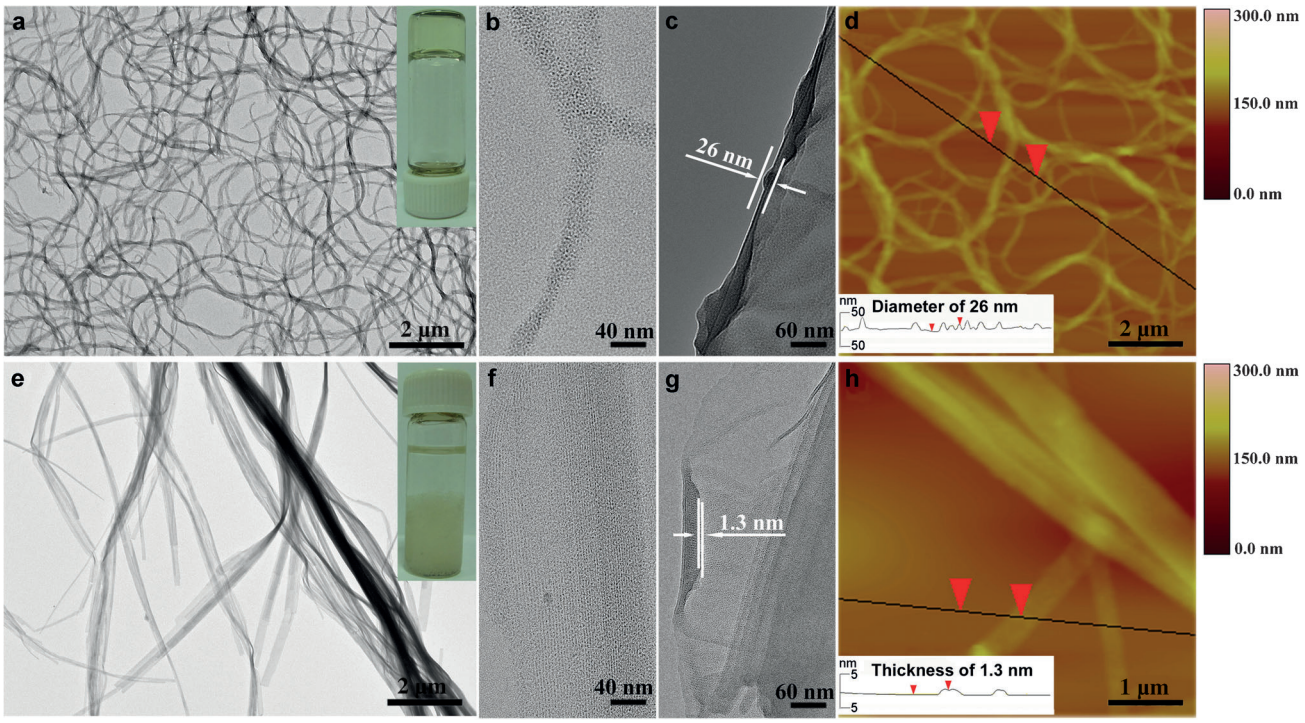

Figure 2. TEM (a–c, e–g) and tapping-mode AFM (d, h) images of Wire-26 (a–d) and Ribbon-1.3 (e–h). TEM images of a small region of Wire-26 and Ribbon-1.3 oriented parallel to (b, f) and vertical on (c, g) the TEM grid are indicated. Inset in (a): image showing the formation of a viscous gel upon assembly of $Cu_{12}DT_8Ac_4$ NCs into Wire-26. Inset in (e): image showing Ribbon-1.3 in colloidal solution.

consistent with the TEM-measured diameter of the NWs vertical to the TEM grid (Figure 2c). MALDI-TOF mass spectrometry and energy-dispersive X-ray spectroscopy (EDS) reveal that the Cu NCs within Wire-26 are composed of $Cu_{12}DT_8Ac_4$ (Figure 3a and Figure S3, respectively). X-ray photoelectron spectroscopy (XPS) of the Cu LMM peak confirms the coexistence of Cu^0 and Cu^I in $Cu_{12}DT_8Ac_4$, containing 8 Cu^I atoms and 4 Cu^0 atoms (Figure S4). This composition is attributed to the coordination of DT and Ac to the Cu atoms. The DT has a stronger coordination interaction with the Cu center through a Cu–S bond, whereas the Cu–O bond between the Cu center and the Ac is much weaker. Thus, the Cu–DT coordination results in a copper valence of Cu^I, and for the Cu–Ac a valence of Cu^0 is evident for the Cu center. Upon annealing Wire-26 at 120 °C for 30 minutes, a dramatic decrease of the thickness from 26 to 1.3 nm is measured by TEM and AFM (Figures 2e–h and Figure S2 in the Supporting Information), producing Ribbon-1.3 with an approximate width of 50–400 nm and a length of about 100 μm. In contrast to Wire-26, the diameter of NCs within Ribbon-1.3 decreases from 1.9 to 1.3 nm (Figure 2f and Figure S1). MALDI-TOF mass spectrometry indicates a composition change from $Cu_{12}DT_8Ac_4$ to

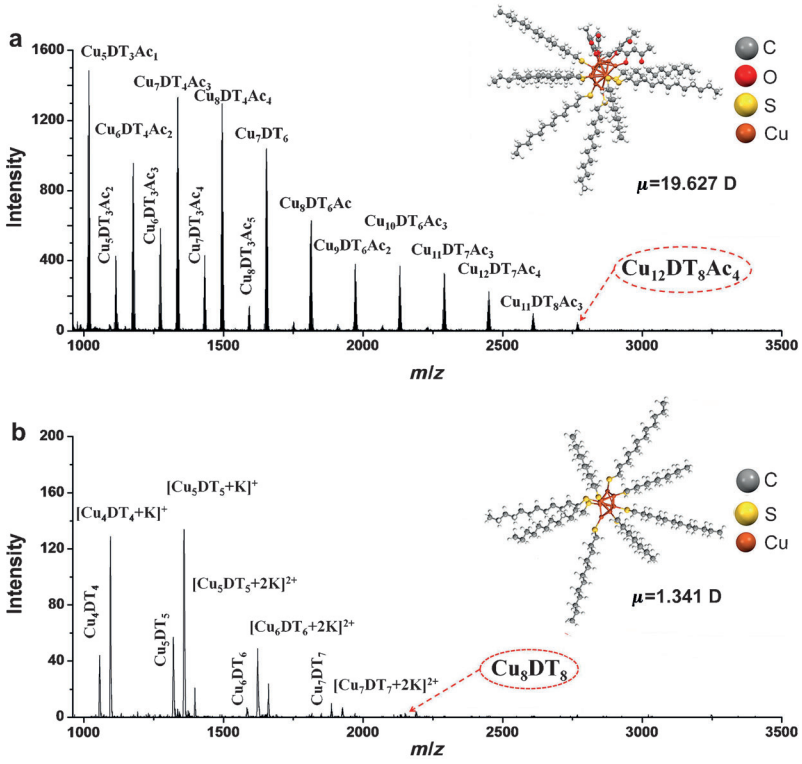

Figure 3. The MALDI-TOF mass spectra of a) Wire-26 and b) Ribbon-1.3, showing compositions of $Cu_{12}DT_8Ac_4$ (a) and Cu_8DT_8 (b). Insets in (a) and (b): computer-optimized structures of $Cu_{12}DT_8Ac_4$ (a) and Cu_8DT_8 (b) used to calculate the permanent dipole moment μ of each.

Cu_8DT_8 (Figure 3). Differential thermal gravimetric analysis and FTIR data also demonstrate the loss of the Ac after annealing (Figures S5 and S6). Both Wire-26 and Ribbon-1.3 exhibit strong luminescence, implying that they are composed of self-assembled Cu NCs (Figure S7). The NCs within Ribbon-1.3 have an ordered hexagonal arrangement with an average distance of 2.9 nm (Figure 2 f). This distance is in good agreement with the previously reported NC self-assembled architectures.[5f]

The self-assembly of $Cu_{12}DT_8Ac_4$ NCs into Wire-26 is a low-temperature kinetically controlled process.[6] The formation of Wire-26 can occur in a temperature range of 25–80 °C. Use of temperatures at the higher end of this range only accelerates the self-assembly. To investigate the intermediate steps, the self-assembly process was monitored by TEM at 30 °C (Figure S8). In general, the self-assembly is quite fast and Wire-26 can form within 10 minutes. After injection of the DT for 1 minute, $Cu_{12}DT_8Ac_4$ NCs with an average diameter of 2.0 nm form first (Figures S8 and S9). By considering the specific arrangement of the Cu atoms in the NCs, the conformation of the NCs, and the distribution of DT on the NC surface,[7] computer-aided calculations reveal that the permanent dipole moment of $Cu_{12}DT_8Ac_4$ is as high as 19.627 D (Figure S10). The energy of dipolar attraction afforded by a permanent dipole moment of 19.627 D is 10.86 kJ mol^{-1} (Figure S11), which is substantially higher than the energy (1.5 kJ mol^{-1}) of regular molecular dipole–dipole attractions.[5b] Driven by the strong dipolar attraction, a one-dimensional (1D) orientated self-assembly of Cu NCs into NWs is initiated (Figure S8). Additionally, the vdW attraction between the DT molecules on Cu NCs further reinforce the self-assembled architectures. The length of the DT alkyl chain is 1.7 nm when elongated,[8] which generates strong vdW interactions between the NCs within Wire-26. The vdW attraction between the neighboring $Cu_{12}DT_8Ac_4$ NCs is calculated to be 4.1 k_BT, where k_B is the Boltzmann constant and T is the absolute temperature (Figure S12). Further computer simulations on the formation of Wire-26 were carried out on the basis of Brownian dynamics using a coarse-grained model (Figure S13).[9] The simulated result is consistent with the experimental observation.

As $Cu_{12}DT_8Ac_4$ NCs assemble into Wire-26, the initial pale-yellow solution becomes turbid and a viscous gel forms (Figure 2 a, inset, and Figure S14), showing the strong interactions between individual Wire-26 NWs. For microscale hydrophobic structures, vdW attraction is the major interaction.[10] Additionally, prolonged annealing of Wire-26 at 30 °C for 30 minutes leads to structural reorganization into flowerlike architectures (Figure S15). This means that Wire-26 is thermodynamically unstable, providing a means for further structural control.

At the higher annealing temperature of 120 °C, ultrathin ribbons with a thickness of approximately 1.3 nm are obtained. TEM measurements confirm the temporal evolution of Ribbon-1.3 from Wire-26 (Figure S16). As a result of the strong vdW interactions, Ribbon-1.3 forms free-standing architectures and can be collected for further applications (Figure 2 e and Figure S17). In the evolution of the structure, the quantity of DT added to the reaction is an important factor (Figure S18). In a typical experiment, Ribbon-1.3 is not formed until the quantity of added DT is higher than 0.03 mL (0.12 mmol). Increasing the quantity of DT added can accelerate the structural evolution towards Ribbon-1.3, implying the correlation of an intrinsic driving force with DT. In this scenario, DT facilitates the removal of the Ac from $Cu_{12}DT_8Ac_4$, enabling the conversion into Cu_8DT_8 (Figure 3). This process decreases the complexity of building blocks during structural reorganization, and improves the compactness and order of NC arrangement in Ribbon-1.3 (Figures 2 b and f), which is confirmed by small-angle X-ray powder diffraction (Figure S19).

Computer-aided calculations indicate that the permanent dipole moment of Cu_8DT_8 NCs is only 1.341 D as a result of its good structural symmetry (Figure S10). The corresponding energy of dipolar attraction is quite low (0.24 kJ mol^{-1}), enabling removal of the Ac (Figure S11). Most importantly, the significant decrease of Cu_8DT_8 dipolar attraction in comparison to $Cu_{12}DT_8Ac_4$ breaks the cooperation between dipolar and vdW attraction within NCs, thus permitting the reorganization of preassembled NCs. This reorganization occurs in the two miscible solvents BE and LP which have a slight polarity difference. Under annealing conditions, their microphase separation generates a lamellar interface, which acts as soft template to direct the reorganization with 2D orientation.[8] Additionally, there is a temperature barrier (120 °C in our experiments) to the formation of Ribbon-1.3. In this context, the DT vdW attraction between neighboring NCs provides the main driving force for NC reorganization. The vdW attraction between the Cu_8DT_8 NCs is calculated to be 3.8 k_BT (Figure S12). At elevated temperature, the mobility of DT alkyl chains within the self-assembled structures is rather dynamic, thus driving the NCs to form a compact and ordered array.[11]

The electrocatalytic properties of isolated Cu NCs, Wire-26, and Ribbon-1.3 as cathode catalysts for ORR are compared by cyclic voltammetry. In general, Wire-26 and Ribbon-1.3 retain the electrocatalytic activity of Cu NCs (Figure 4 a). The current density of Ribbon-1.3 is higher than Wire-26 and then isolated NCs, because of the self-assembly features of nanoribbons. TEM images show that the isolated NCs strongly tend to aggregate during the catalytic reaction, whereas both the NWs and ribbons do not (Figure S20). This is the reason that Wire-26 and Ribbon-1.3 exhibit higher current densities, because a larger surface area is preserved. To gain further insight, the reaction kinetics of different catalysts is revealed by rotating-disk voltammetry (Figure 4 b). For Ribbon-1.3, the oxygen reduction current density recorded at the glassy-carbon electrode increases as the rotation speed increases from 225 to 2500 rpm. The Koutecky–Levich plots at different electrode potentials indicate good linearity over the range from −1.05 to −0.7 V, from which the number of transferred electrons (n) per oxygen molecule are calculated (Figure S21). The n value calculated for Ribbon-1.3 is 2.5–3.6, which is much higher than Wire-26 ($n = 2.2$) and isolated NCs ($n = 1.5$–2.0) (Figure 4 c, S22 and S23). This confirms that Ribbon-1.3 composed of Cu_8DT_8 is more active than Wire-26 and isolated Cu NCs composed of $Cu_{12}DT_8Ac_4$.

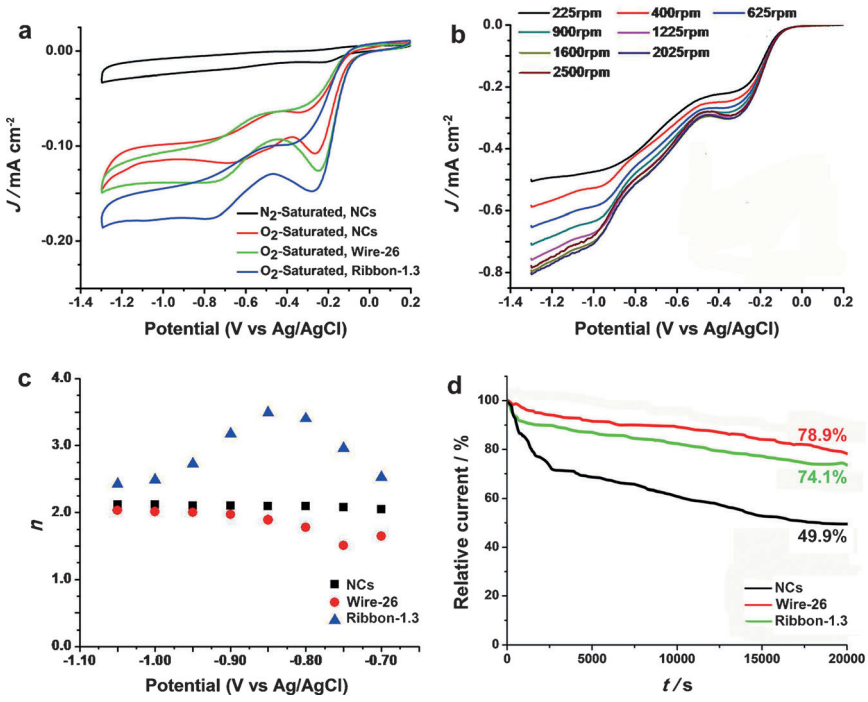

Figure 4. a) Cyclic voltammograms of isolated Cu NCs for ORR in O_2- and N_2-saturated solutions of KOH (0.1 M), and Wire-26 and Ribbon-1.3 for ORR in O_2-saturated solutions of KOH (0.1 M). The quantity of catalysts on electrodes is fixed at 5 mg mL^{-1}. b) Rotating-disk voltammograms recorded for Ribbon-1.3 supported on a bare glassy-carbon electrode in an O_2-saturated KOH solution (0.1 M) at a scan rate of 50 mV s^{-1} and different rotation rates. c) The dependence of the number of transferred electrons (n) on the applied electrode potentials, ranging from −1.05 to −0.7 V for isolated NCs, Wire-26, and Ribbon-1.3. d) Current–time chronoamperometric response of isolated NCs, Wire-26, and Ribbon-1.3 at −0.7 V in O_2-saturated KOH solution (0.1 M) at a rotation rate of 1600 rpm.

Another important issue for ORR catalysts is the durability. The stability of isolated Cu NCs, Wire-26, and Ribbon-1.3 is tested at a constant voltage of −0.7 V for 20000 seconds in an oxygen-saturated KOH solution (0.1 M) at a rotation rate of 1600 rpm (Figure 4d). The current–time chronoamperometric response of Wire-26 and Ribbon-1.3 exhibits a very slow attenuation. After 20000 s, 78.9% and 74.1%, respectively, of the current remained. In contrast, isolated Cu NCs showed a quicker current decrease, with just 49.9% of the current preserved. The improved durability of Cu NCs after assembly is attributed to the anchorage of NCs and/or DT ligands in ultrathin structures, which suppress the isotropic aggregation and fusion of NCs. Additionally, despite the fact that the reduction current density of both isolated Cu NCs and their self-assembled structures are lower than that of the commercial 20% Pt-C catalyst, the onset potentials of O_2 reduction are higher (Figure 4 and Figures S22–24). The durability of NC self-assembled architectures is better than that of the commercial Pt-C catalyst, despite the poorer durability of the unassembled Cu NCs.

In summary, we demonstrate the 2D self-assembly method to improve the durability of catalytic Cu NCs. This method involves the successive formation of $Cu_{12}DT_8Ac_4$ NCs, preassembly of the NCs into NWs, conversion of $Cu_{12}DT_8Ac_4$ into Cu_8DT_8, and the production of thin ribbons through NC reorganization. The cooperation between the dipolar attraction between Cu NCs and the vdW attraction between DT ligands are key driving forces of the self-assembly process. The strong dipolar attraction between $Cu_{12}DT_8Ac_4$ NCs induces their orientated self-assembly to form NWs, and the self-assembly architectures are reinforced by the inter-NC vdW attraction. Further annealing at higher temperature leads to the removal of the Ac ligand from $Cu_{12}DT_8Ac_4$ to form the smaller Cu_8DT_8. This breaks the cooperation between dipolar and vdW forces, and leads to the reorganization of preassembled NCs. As a result, ultrathin ribbons with single NC thickness are produced. Owing to the strong vdW interactions, the ribbons form free-standing architectures and can be collected for catalytic applications. In comparison to isolated Cu NCs, the ribbons exhibit excellent electrocatalytic activity and improved durability.

Received: July 19, 2014
Revised: August 19, 2014
Published online: September 15, 2014

Keywords: copper · electrocatalysis · nanostructures · oxygen reduction reaction · self-assembly

[1] a) W. Chen, S. W. Chen, *Angew. Chem. Int. Ed.* **2009**, *48*, 4386–4389; *Angew. Chem.* **2009**, *121*, 4450–4453; b) H. J. Yin, H. J. Tang, D. Wang, Y. Gao, Z. Y. Tang, *ACS Nano* **2012**, *6*, 8288–8297; c) W. T. Wei, Y. Z. Lu, W. Chen, S. W. Chen, *J. Am. Chem. Soc.* **2011**, *133*, 2060–2063; d) W. J. Zhou, X. J. Wu, X. H. Cao, X. Huang, C. L. Tan, J. Tian, H. Liu, J. Y. Wang, H. Zhang, *Energy Environ. Sci.* **2013**, *6*, 2921–2924; e) X. Huang, C. L. Tan, Z. Y. Yin, H. Zhang, *Adv. Mater.* **2014**, *26*, 2185–2204; f) J. X. Zhu, D. Yang, Z. Y. Yin, Q. Y. Yan, H. Zhang, *Small* **2014**, *10*, 3480–3498.

[2] S. J. Guo, S. Zhang, S. H. Sun, *Angew. Chem. Int. Ed.* **2013**, *52*, 8526–8544; *Angew. Chem.* **2013**, *125*, 8686–8705.

[3] a) A. Corma, P. Concepción, M. Boronat, M. J. Sabater, J. Navas, M. J. Yacaman, E. Larios, A. Posadas, M. A. López-Quintela, D. Buceta, E. Mendoza, G. Guilera, A. Mayoral, *Nat. Chem.* **2013**, *5*, 775–781; b) C. Jeyabharathi, S. S. Kumar, G. V. M. Kiruthika, K. L. N. Phani, *Angew. Chem. Int. Ed.* **2010**, *49*, 2925–2928; *Angew. Chem.* **2010**, *122*, 2987–2990.

[4] Y. Z. Lu, W. Chen, *Chem. Soc. Rev.* **2012**, *41*, 3594–3623.

[5] a) Z. Y. Tang, Z. L. Zhang, Y. Wang, S. C. Glotzer, N. A. Kotov, *Science* **2006**, *314*, 274–278; b) Z. Y. Tang, N. A. Kotov, M. Giersig, *Science* **2002**, *297*, 237–240; c) Y. S. Xia, T. D. Nguyen, M. Yang, B. Lee, A. Santos, P. Podsiadlo, Z. Y. Tang, S. C. Glotzer, N. A. Kotov, *Nat. Nanotechnol.* **2011**, *6*, 580–587; d) Y. Gao, Z. Y. Tang, *Small* **2011**, *7*, 2133–2146; e) Y. S. Xia, Z. Y. Tang, *Adv. Funct. Mater.* **2012**, *22*, 2585–2593; f) Y. S. Xiong, K. Deng, Y. Y. Jia, L. C. He, L. Chang, L. J. Zhi, Z. Y. Tang, *Small* **2014**, *10*, 1523–1528.

[6] X. Q. Huang, S. H. Tang, X. L. Mu, Y. Dai, G. X. Chen, Z. Y. Zhou, F. X. Ruan, Z. L. Yang, N. F. Zheng, *Nat. Nanotechnol.* **2011**, *6*, 28 – 32.
[7] P. Calaminici, M. Pérez-Romero, J. M. Vásquez-Pérez, A. M. Köster, *Comput. Theor. Chem.* **2013**, *1021*, 41 – 48.
[8] Z. N. Wu, C. W. Dong, Y. C. Li, H. X. Hao, H. Zhang, Z. Y. Lu, B. Yang, *Angew. Chem. Int. Ed.* **2013**, *52*, 9952 – 9955; *Angew. Chem.* **2013**, *125*, 10136 – 10139.
[9] Y. L. Zhu, H. Liu, Z. W. Li, H. J. Qian, G. Milano, Z. Y. Lu, *J. Comput. Chem.* **2013**, *34*, 2197 – 2211.
[10] a) S. Ithurria, M. D. Tessier, B. Mahler, R. P. S. M. Lobo, B. Dubertret, A. L. Efros, *Nat. Mater.* **2011**, *10*, 936 – 941; b) Y. H. Liu, F. D. Wang, Y. Y. Wang, P. C. Gibbons, W. E. Buhro, *J. Am. Chem. Soc.* **2011**, *133*, 17005 – 17013; c) J. Yang, J. S. Son, J. H. Yu, J. Joo, T. Hyeon, *Chem. Mater.* **2013**, *25*, 1190 – 1198.
[11] a) Y. P. Du, Z. Y. Yin, J. X. Zhu, X. Huang, X. J. Wu, Z. Y. Zeng, Q. Y. Yan, H. Zhang, *Nat. Commun.* **2012**, *3*, 1177; b) S. Acharya, S. Sarkar, N. Pradhan, *J. Phys. Chem. Lett.* **2012**, *3*, 3812 – 3817.

